Journal of Alloys and Compounds 509 (2011) 4839–4847

Contents lists available at ScienceDirect

Journal of Alloys and Compounds

journal homepage: www.elsevier.com/locate/jallcom

Corrosion resistance of Mg–5Al–*x*Sr alloys

N.D. Nam[a], W.C. Kim[a], J.G. Kim[a,*], K.S. Shin[b], H.C. Jung[b]

[a] Department of Advanced Materials Science and Engineering, Sungkyunkwan University, 300 Chunchun-Dong, Jangan-Gu, Suwon 440-746, Republic of Korea
[b] Magnesium Technology Innovation Center, School of Materials Science and Engineering, Seoul National University, Seoul 151-744, Republic of Korea

ARTICLE INFO

Article history:
Received 19 August 2010
Received in revised form 24 January 2011
Accepted 27 January 2011
Available online 23 February 2011

Keywords:
Magnesium alloy
EIS
Polarization
Alkaline corrosion
Passive film
Pitting corrosion

ABSTRACT

Four types of Mg–5Al alloy with various weight percentages of Sr ranging from 0 to 1.5 wt% were examined using electrochemical techniques and surface analyses. The electrochemical results indicated that the Mg–5Al alloy containing Sr to have a higher pitting potential and impedance than the Mg–5Al specimen with highest value being observed in the Mg–5Al–1Sr specimen. Sr addition induced the continuous precipitation of Al–Sr phases along with grain refinement and increased the formation of an $Al(OH)_3$ film on the surface.

1. Introduction

Mg and its alloys are lightweight with low density. In addition, they exhibit electromagnetic wave shielding, stiffness, heat/creeping resistance, surface quality, formability, energy absorption, strength, and high fracture elongation in power-train components, where large die-cast components are used in the automotive, aerospace and electronic industries [1–7]. To increase its applications, Agnewa and Nie [8] suggested the following four major areas of research: (i) use of the computational materials science and engineering approaches in alloy development including thermodynamic and first-principles modeling; (ii) mechanistic understanding and development of creep-resistant casting alloys; (iii) mechanistic understanding and modeling of deformation, including mechanical twinning and dynamic recrystallization; and (iv) texture modification via alloying and processing, particularly strip casting of the sheet. This is a perspective for future research to improve the properties and broaden the structural applications of magnesium alloys.

Magnesium alloys have the disadvantage of poor corrosion resistance and low formability [9]. Therefore, a further requirement in recent years has been superior corrosion performance. Dramatic improvements in corrosion performance have been demonstrated in new magnesium alloys. Improvements in the mechanical properties and corrosion resistance have led to greater interest in magnesium alloys for aerospace and special applications. For this reason, many studies focused on improving the mechanical and corrosion properties of Mg alloys to achieve the excellent corrosion resistance and mechanical properties needed for industrial applications [10–31].

Mg and its alloys form MgO or $Mg(OH)_2$ passive films on their surface. However, MgO can crack easily and $Mg(OH)_2$ can roll up due to residual stress [32,33]. Therefore, the composition and structure of the oxide/hydroxide film are often reinforced by adding an active metal [34–38], such as aluminum [39], or a heavy metal (such as iron and nickel) [40–50]. However, precipitates, such as heavy metal-magnesium compounds, act as local cathodes during corrosion [51], which has prompted the development of low heavy metal content alloys. The rapid solidification process refines the microstructure to optimize the composition, which improves the corrosion resistance, creep resistance, tensile yield strength and castability. This process also allows for the addition of more active elements with similar reduction potentials to Mg, such as alkaline [52] and rare earth [53–62] alloying additions.

Al-containing Mg alloys feature a thinner film with a density that increases with increasing Al content. The surface film of Al-containing alloys contains a mixture of MgO and Al_2O_3 or $Mg(OH)_2$ and $Al(OH)_3$. The presence of Al in the passive layer ameliorates its protective behavior [63–66]. However, Al only improves the corrosion resistance of Mg alloys at high concentrations. Therefore, the effect of a small amount (such as 5 wt%) of aluminum in the Mg alloy is still questionable. Cho et al. [67] reported that Mg alloyed with 5% Al includes both α-Mg and β-$Mg_{17}Al_{12}$ phases. Furthermore, a Mg–5Al alloy containing Sr showed supe-

* Corresponding author. Tel.: +82 312907360; fax: +82 312907371.
E-mail address: kimjg@skku.ac.kr (J.G. Kim).

0925-8388/$ – see front matter © 2011 Elsevier B.V. All rights reserved.
doi:10.1016/j.jallcom.2011.01.187

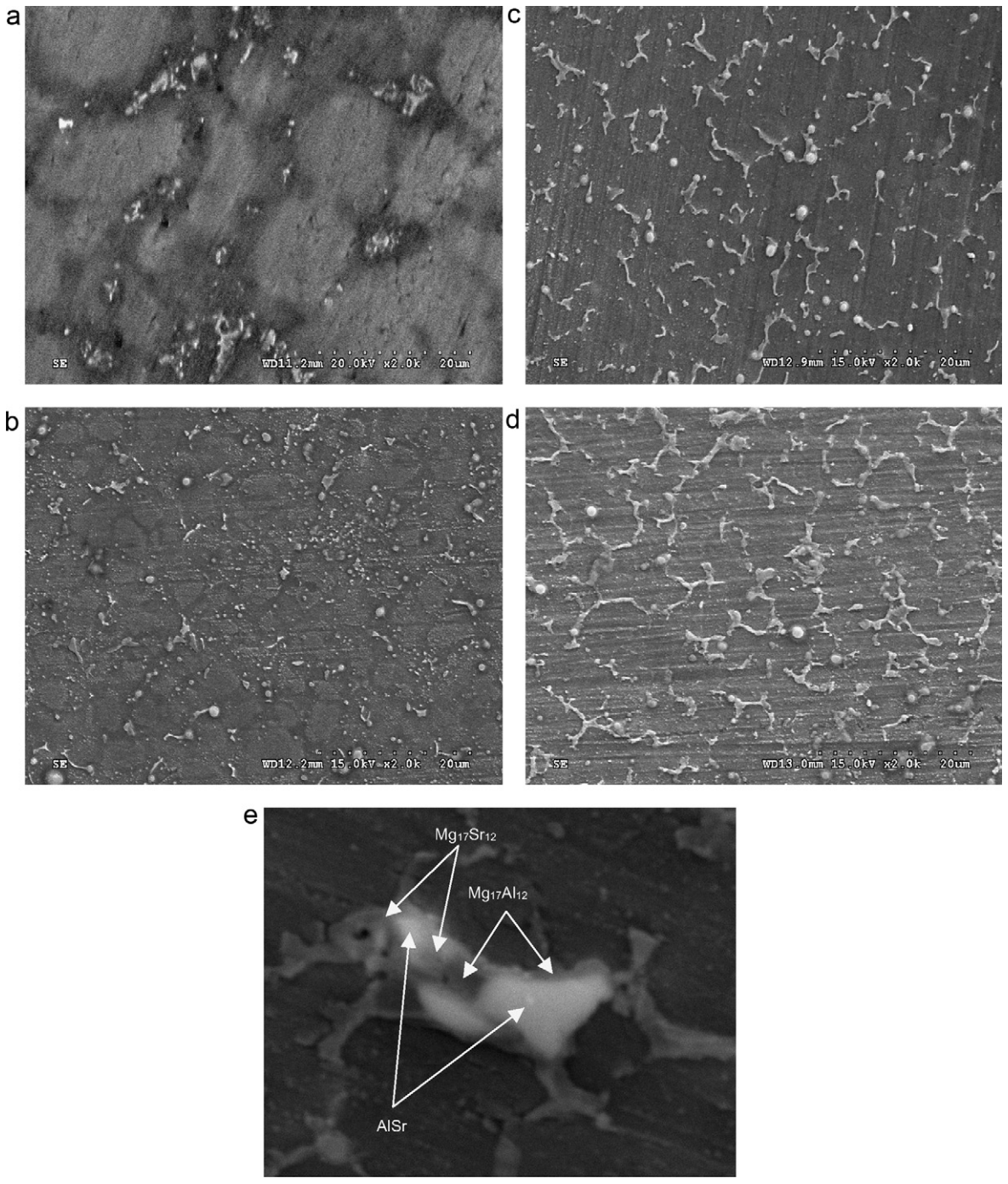

Fig. 1. SEM images of the die-cast alloys: (a) Mg–5Al, (b) Mg–5Al–0.5Sr, (c) Mg–5Al–1.0Sr, (d) Mg–5Al–1.5Sr, and (e) $Mg_{17}Al_{12}$ and phase containing Sr of Sr-containing specimens.

rior creep resistance, excellent high-temperature properties and good castability [68–71]. In addition, Sr is beneficial in improving the corrosion resistance of Mg alloys [72–77]. The creep resistance of Mg–5Al–2Sr was suggested to be related to the low aluminum supersaturation of primary magnesium and the absence of an $Mg_{17}Al_{12}$ phase.

A small grain size, higher precipitation density, more continuous over the Mg matrix, and improved corrosion resistance were observed when mischmetal (Mm) was added to the Mg–5Al alloy. However, the effects of Mm addition are still questionable in the higher potential region due to pitting corrosion [78]. This article reports the corrosion properties and passive ability of the Mg–Al–*x*Sr (x = 0–1.5 wt%) alloy series. The microstructure and corrosion properties were evaluated as a function of the alloy composition using electrochemical techniques in a 0.01 M NaCl (pH = 12) as an alkaline solution [79] and surface analysis methods.

Table 1
Nominal composition (in wt%) of the alloy investigated.

Samples	Composition (wt%)
# 1	5 Al, 0.0 Sr, bal Mg
# 2	5 Al, 0.5 Sr, bal Mg
# 3	5 Al, 1.0 Sr, bal Mg
# 4	5 Al, 1.5 Sr, bal Mg

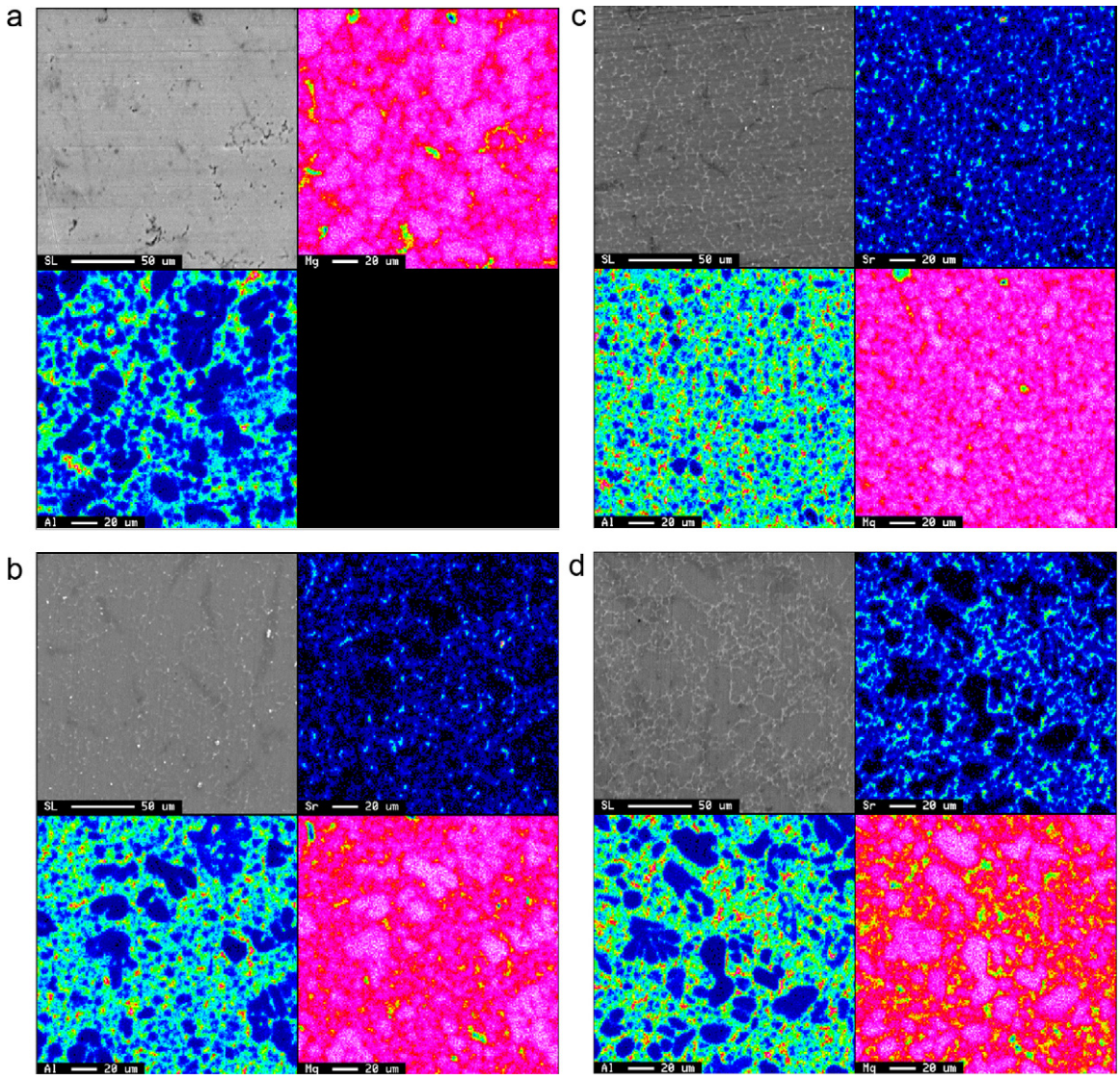

Fig. 2. EPMA map of the alloying elements on the specimen surfaces: (a) Mg–5Al, (b) Mg–5Al–0.5Sr, (c) Mg–5Al–1.0Sr, and (d) Mg–5Al–1.5Sr.

2. Experimental procedures

2.1. Specimen preparation

All Mg–5Al–*x*Sr (*x* = 0, 0.5, 1.0, and 1.5) alloys were die-cast on a 320-ton high pressure die casting machine. Table 1 lists the alloy designation and corresponding chemical composition of each alloy. All specimens were cut from the same location of each die-cast specimen. The specimens were finished by grinding with 800-grit silicon carbide (SiC) paper. For the microstructure observations, the die-cast specimens were polished mechanically with SiC paper (#2000) and then with 1 μm alumina powder. The specimens were then etched in 0.008 mol/dm^3 HNO_3 for 10 s.

2.2. Electrochemical investigation methods

All electrochemical experiments were carried out at room temperature in a 0.01 M NaCl solution (pH = 12 ± 0.0001). The exposed coating area was

Table 2
Electrochemical corrosion characteristics in 0.01 M NaCl (pH = 12) solution.

	E_{corr} (mV_{SCE})	E_{pit} (mV_{SCE})	$E_{pit} - E_{corr}$ (mV_{SCE})
Mg–5Al	−1127.44	−875.63	251.81
Mg–5Al–0.5Sr	−1180.72	−670.12	510.60
Mg–5Al–1.0Sr	−1202.02	1300.05	2502.07
Mg–5Al–1.5Sr	−1228.64	730.53	1959.17

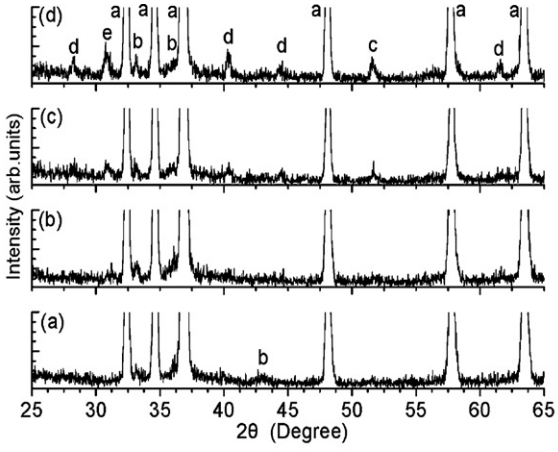

(a) Mg-5Al, (b) Mg-5Al-0.5Sr, (c) Mg-5Al-1.0Sr, and (d) Mg-5Al-1.5Sr; a, Mg; b, $Mg_{17}Al_{12}$; c, $Mg_{17}Sr_{12}$; d, Al_4Sr; e, AlSr.

Fig. 3. XRD patterns of the Mg–5Al alloys.

1 cm^2. Before each experiment, oxygen was removed from the solution by bubbling with nitrogen for 2 h. A potentiodynamic polarization test was performed using an EG&G PAR 263A for the DC measurements with a graphite counter electrode and a saturated calomel electrode as a reference. Before the potentiodynamic polarization test, the specimens were kept in solution for 2 h to stabilize the open-circuit potential. The potential of the electrodes was swept from −250 mV versus E_{corr} to 1600 mV$_{SCE}$ at a rate 0.166 mV/s. Potentiostatic tests were carried out to examine the tendency of passive film breakdown (pit initiation and propagation) as a function of the Sr content. Electrochemical impedance spectroscopy (EIS) was performed using a Zahner IM6e system with a commercial software program for the AC measurements. The amplitude of sinusoidal perturbation was 10 mV. The frequency range ranged from 100 kHz to 10 mHz. The tests were conducted every 24 h over a period of 7 days.

2.3. Surface analyses

The crystal structure of the as-received specimens was examined by X-ray diffraction (XRD) using Cu K_α radiation. The corresponding microstructures were observed by electron probe microanalysis (EPMA) after polishing with 1 μm alumina powder, and scanning electron microscopy (SEM) after etching in a 0.008 mol/dm^3 HNO_3 solution. The relationship between the electrochemical behavior and surface morphology of pitting was examined by SEM after applying a potential. The passive film was examined by X-ray photoelectron spectroscopy (XPS) after the passive film had become stable and enriched by passive potential application.

3. Results and discussion

3.1. Structure and composition

Fig. 1 shows the grain morphology of the Mg–5Al–*x*Sr alloys after etching in 0.008 mol/dm^3 HNO_3. The microstructures consisted of an α-Mg matrix along with precipitates of $Mg_{17}Al_{12}$ and/or Sr-containing compounds along the grain boundaries. The grain size of the Mg–5Al specimen without Sr addition was large (Fig. 1(a)) with the formation of a few precipitates with discontinuity. For the specimens containing 0.5, 1.0 and 1.5 wt% Sr, the grain size was refined, and more continuous precipitates formed along the grain boundaries, particularly in the case of 1.0 and 1.5 wt% Sr addition. However, for the alloys containing 1.5 wt% Sr, an excess of 1.0 wt% Sr will react with Mg to form $Mg_{17}Sr_{12}$ phases instead of Al–Sr phases, which are commonly observed in commercial Mg–Al based alloys. This limits the solid solubility of the Sr solute in magnesium. Therefore, the rapid enrichment of Sr in the liquid ahead of the growing interface will prefer precipitated limb growth during solidification. Therefore, complex precipitates are observed in Fig. 1(d). A detailed microscopy examination was carried out on the Mg–5Al–*x*Sr alloys using EPMA mapping after micropolishing. EPMA analysis was performed to determine the elemental distribution of Mg, Al and Sr in the microstructure shown in Fig. 2. High concentrations of Al and Sr were observed in the grain boundary regions, indicating β-$Mg_{17}Al_{12}$ and Sr-containing compounds.

The XRD pattern in Fig. 3 revealed the existence of Mg, $Mg_{17}Al_{12}$, $Mg_{17}Sr_{12}$, Al_4Sr and AlSr phases in the Mg–5Al–*x*Sr alloy. There were no significant differences in the α-Mg peaks between the Mg–5Al and Sr-containing specimens. However, the Sr specimens had Sr-containing phases formed by a reaction of Sr with Al and Mg to form Al–Sr and Mg–Sr phases. This is expected to result in a decrease in the amount of β-$Mg_{17}Al_{12}$ in the specimens containing Sr because the added Sr reacts with Al to form intermetallic compounds, such as Al_4Sr and AlSr. Al–Sr phases were observed in all Sr-containing specimens. The intensities of the Al–Sr diffraction peaks increased with increasing Sr content. Moreover, the addition of Sr also increased the $Mg_{17}Sr_{12}$ phase with increasing Sr content, indicating that an increase in the Sr content enhanced the reaction of Sr with both Mg and Al to form Mg–Sr and Al–Sr phases.

The microstructure of the alloy in the Mg–5Al specimen and those containing Sr was quite different. The Sr-containing specimen consisted of an α-Mg matrix and precipitates of $Mg_{17}Al_{12}$ and/or Sr-containing compounds along the grain boundaries. In particular, the density of the precipitates along the grain boundaries increased with increasing Sr content. The Mg–5Al specimens with Sr addition contained relatively small α-Mg grains; the concentration of the precipitates increased with increasing Sr content. The distribution of precipitates became more continuous in the specimens with increasing Sr content. However, in the 1.5 wt% Sr, a $Mg_{17}Sr_{12}$ phase and precipitated limb growth were observed during solidification. This might affect the corrosion performance because this phase is believed to act as a barrier of a small grain size, higher precipitation density and greater continuity over the Mg matrix.

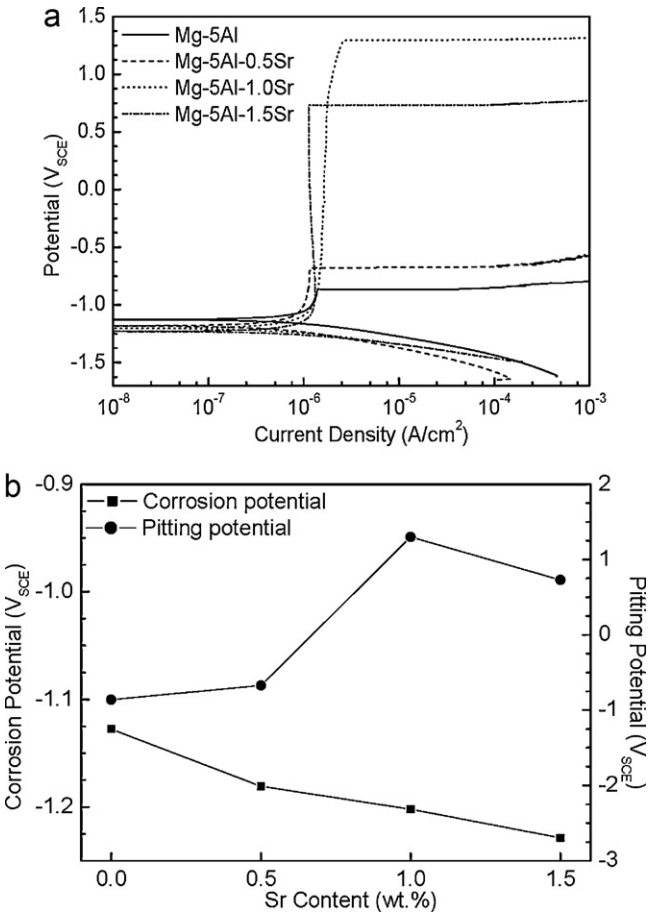

Fig. 4. (a) Polarization curves of Mg–5Al as a function of the Sr content and (b) effect of Sr on the corrosion and pitting potentials of Mg–5Al in a 0.01 M NaCl solution (pH = 12) at room temperature.

3.2. Corrosion resistance

Fig. 4(a) shows the potentiodynamic polarization curves of the Mg–5Al–*x*Sr. Fig. 4(b) presents the measured corrosion potential and pitting potential (E_{pit}). All the alloys were well passivated with a low passive current density, which was related to the very low anodic dissolution of the Sr-containing alloys. The pitting potential increased with increasing Sr content to 1.0 wt% Sr, and then decreased at higher concentrations. The increase in the E_{pit} values with increasing Sr addition suggests that the pitting resistance of the Mg–5Al alloy was improved by the presence of Sr with the highest pitting potential obtained in the case of 1.0 wt% Sr addition as shown in Table 2.

Fig. 5 shows the impedance spectra in the form of the Nyquist plots obtained from the Mg–5Al specimens with Sr contents in a 0.01 M NaCl (pH = 12) solution for 168 h. The semicircular

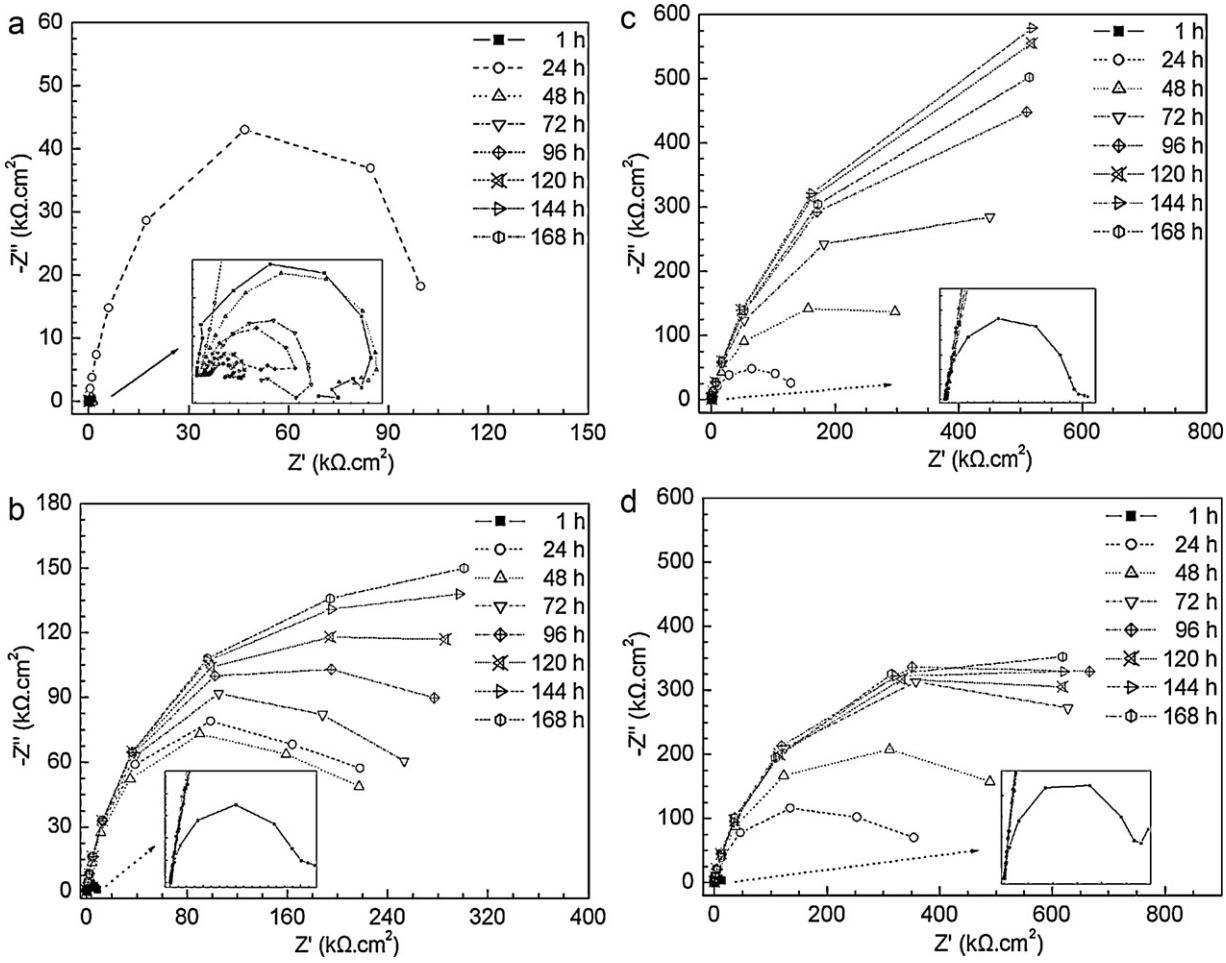

Fig. 5. Nyquist plots of various Mg–5Al alloys.

depression in the Nyquist diagram was attributed to the surface heterogeneity, surface roughness and the existence of two different processes with similar relaxation times. In this study, the surface heterogeneity increased for all specimens due to pitting. The increase in the diameter of the arc suggests improvement in pitting resistance. This indicates that the addition of Sr promotes the formation of a passive film. Fig. 6 also shows the impedance spectra in the form of Bode plots (phase angle versus frequency) during immersion for 168 h at E_{corr}. The high spectrum detects local surface defects, whereas the medium and low frequency spectra detect the process within the film and at the metal/film interface, respectively. The aperture of the phase angles increased with increasing Sr content to 1.0 wt% Sr due to surface film formation, and decreased at higher concentrations. In the case of the Mg–5Al specimen, the phase angles were quite small and the aperture of the phase angles decreased due to pitting. This suggests that Sr addition promotes passive film formation.

The electrochemical response to the impedance tests for the materials under consideration was best simulated using equivalent circuits. Fig. 7 shows the equivalent circuits used for fitting (a) the breakdown film and (b) the passive film, where R_s represents the solution resistance, CPE is the constant phase element, R_p is the polarization resistance, R_{film} is the film resistance, and R_{ct} is the charge transfer resistance. The high-(R_{film}) and low-(R_{ct}) frequency resistance components were affected by the alloying element. In this case, the capacitor was replaced with a CPE to improve the fitting quality, where the CPE contains a double-layer capacitance (C) and phenomenological coefficient (n). The n value of the CPE indicates its meaning: $n = 1$, capacitance; $n = 0.5$, Warburg impedance; $n = 0$, resistance; and $n = -1$, inductance. In this study, n was maintained consistently near 0.8 as a result of the deviation from ideal dielectric behavior. The Zsimpwin program was used to fit the EIS data and determine the optimized values for the resistance parameters (R_{total}), which are shown in Fig. 8. The total resistance increased steadily with increasing immersion time during the initial 168 h. The total resistance (R_{total}) increased strongly with increasing Sr content from the added region to 1.0 wt% Sr due to surface film formation, and decreased with further increases in Sr content. This is important because a high R_{total} value indicates good corrosion resistance.

Fig. 9 presents the results of the potentiostatic test performed at a constant potential of +800 mV_{SCE}. The applied potential was based on the data from the polarization curves in Fig. 4, corresponding to the pitting potential of the Mg–5Al–1.5Sr alloy. The high current density is related to the initiation and propagation of pits. The addition of Sr to the Mg–5Al alloy increased the pitting corrosion resistance, which increased with increasing Sr content to 1.0 wt% Sr and decreased with further increases in Sr content. This corresponds to the results of the polarization test.

Fig. 10 shows the Nyquist plot in the pitting region. +800 mV_{SCE} was applied to all specimens. The impedance diagram spectra obtained in the pitting region represents a single semicircle. Scully et al. [80] reported that the R_p value and depression angle are strongly related to the pitting resistance. Therefore, the surface modification introduced by the formation and propagation of localized pits should be related to the depression angle. Table 3 lists

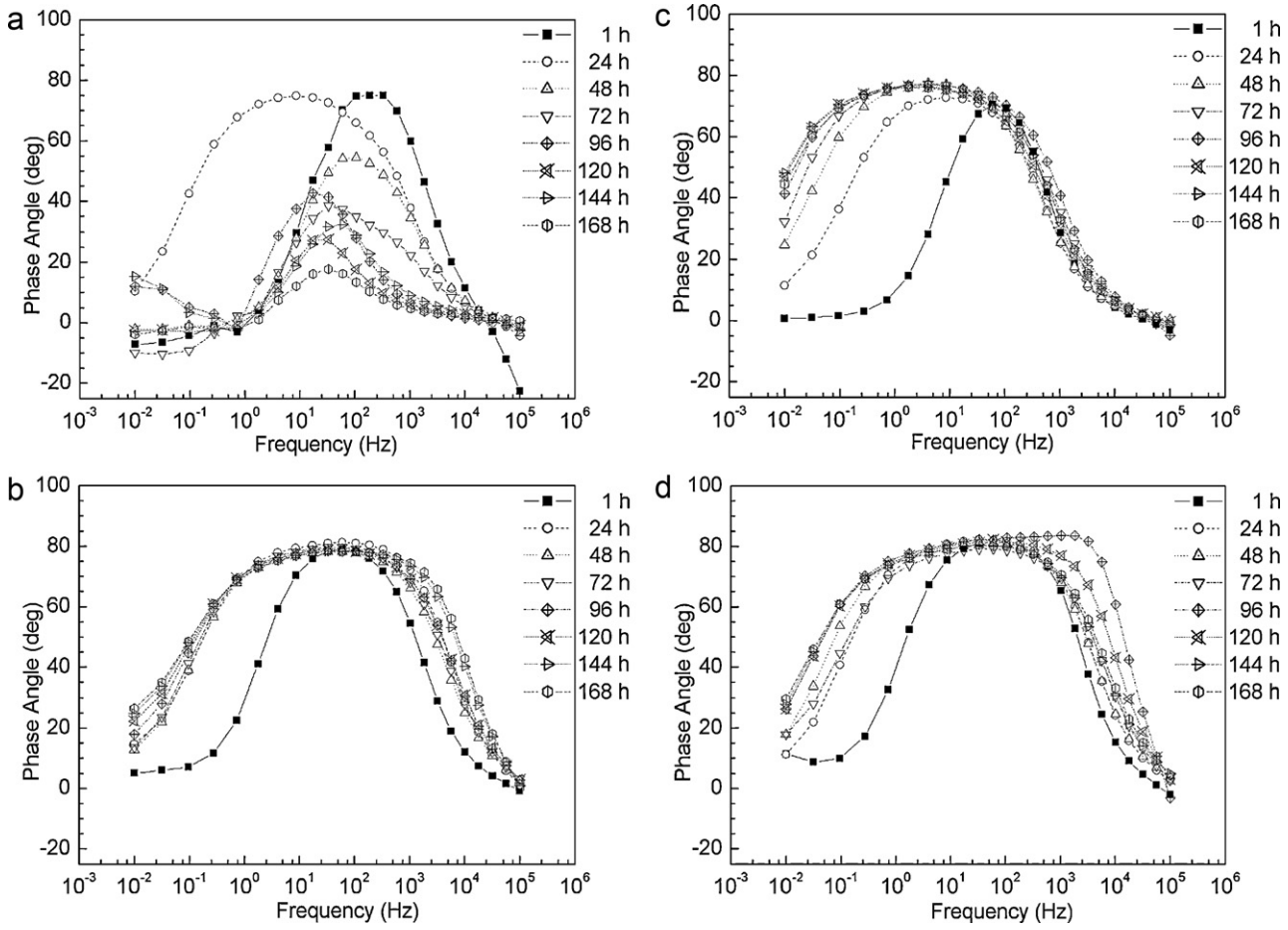

Fig. 6. Bode plots of various Mg–5Al alloys.

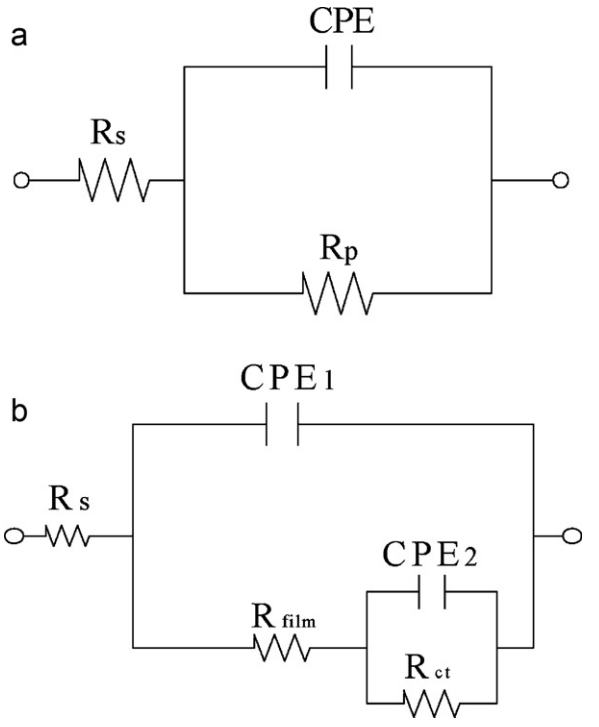

Fig. 7. Equivalent circuit for fitting the EIS data: (a) the breakdown film and (b) passive film on the Mg–5Al–*x*Sr alloy.

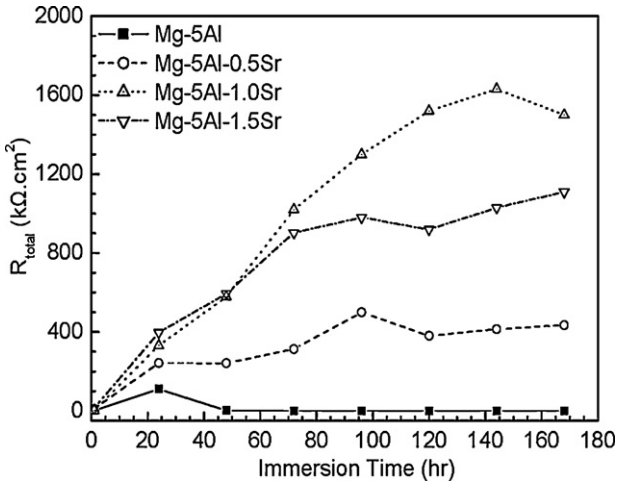

Fig. 8. Effect of the Sr content on R_p in a 0.01 M NaCl solution (pH = 12) at room temperature.

Table 3
EIS results after the application of +800 mV_{SCE}.

	R_p (kΩ cm^2)	Depression angle (°)
Mg–5Al	0.12	−91.68
Mg–5Al–0.5Sr	0.51	−63.99
Mg–5Al–1.0Sr	47.46	−24.63
Mg–5Al–1.5Sr	1.75	−53.62

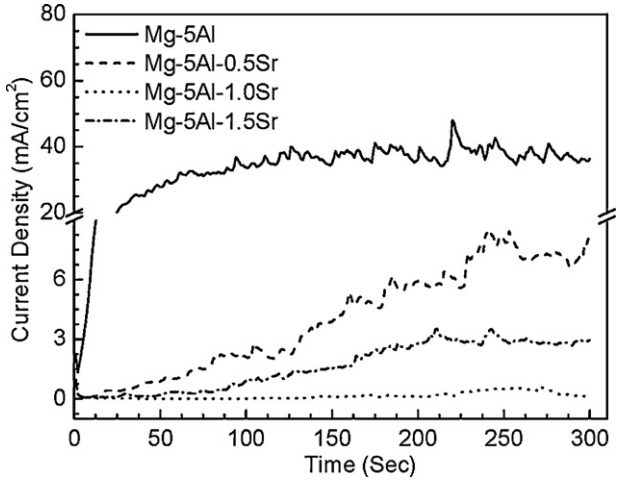

Fig. 9. Changes in the current as a function of time after applying +800 mV_{SCE}.

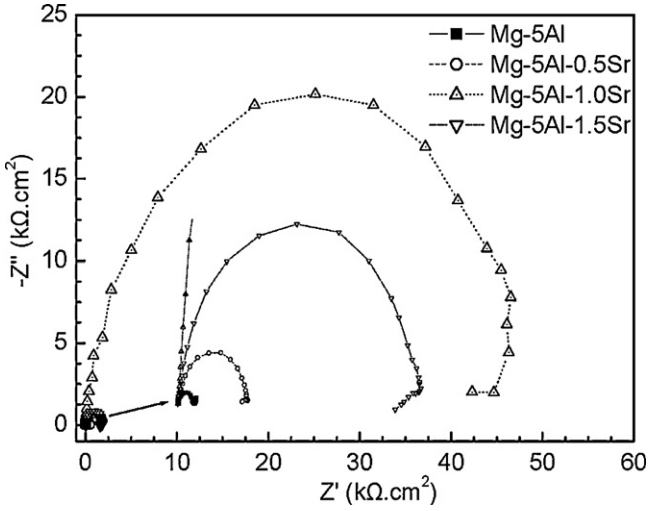

Fig. 10. Impedance spectra of the Nyquist plot of the specimens after the application of +800 mV_{SCE}.

both R_p and the depression angle related to the pitting resistance as a function of the Sr content. The Sr-containing specimens showed higher R_p values, which were obtained from an analysis of the experimental results in Fig. 10, and higher depression angles. In particular, Mg–5Al–1Sr showed the highest depression angle (−24.63°), indicating higher resistance to pitting corrosion.

3.3. Surface analysis after corrosion

Fig. 11 shows SEM images of the surface morphology after the initiation of pitting at 800 mV_{SCE}. No film breakdown was observed on the 1.0 Sr specimens, whereas significant film breakdown was observed on the 0.5, 1.5 wt% Sr and Mg–5Al specimens, as shown in Fig. 11(a), (b) and (d). The film breakdown shown in Fig. 11(a) sug-

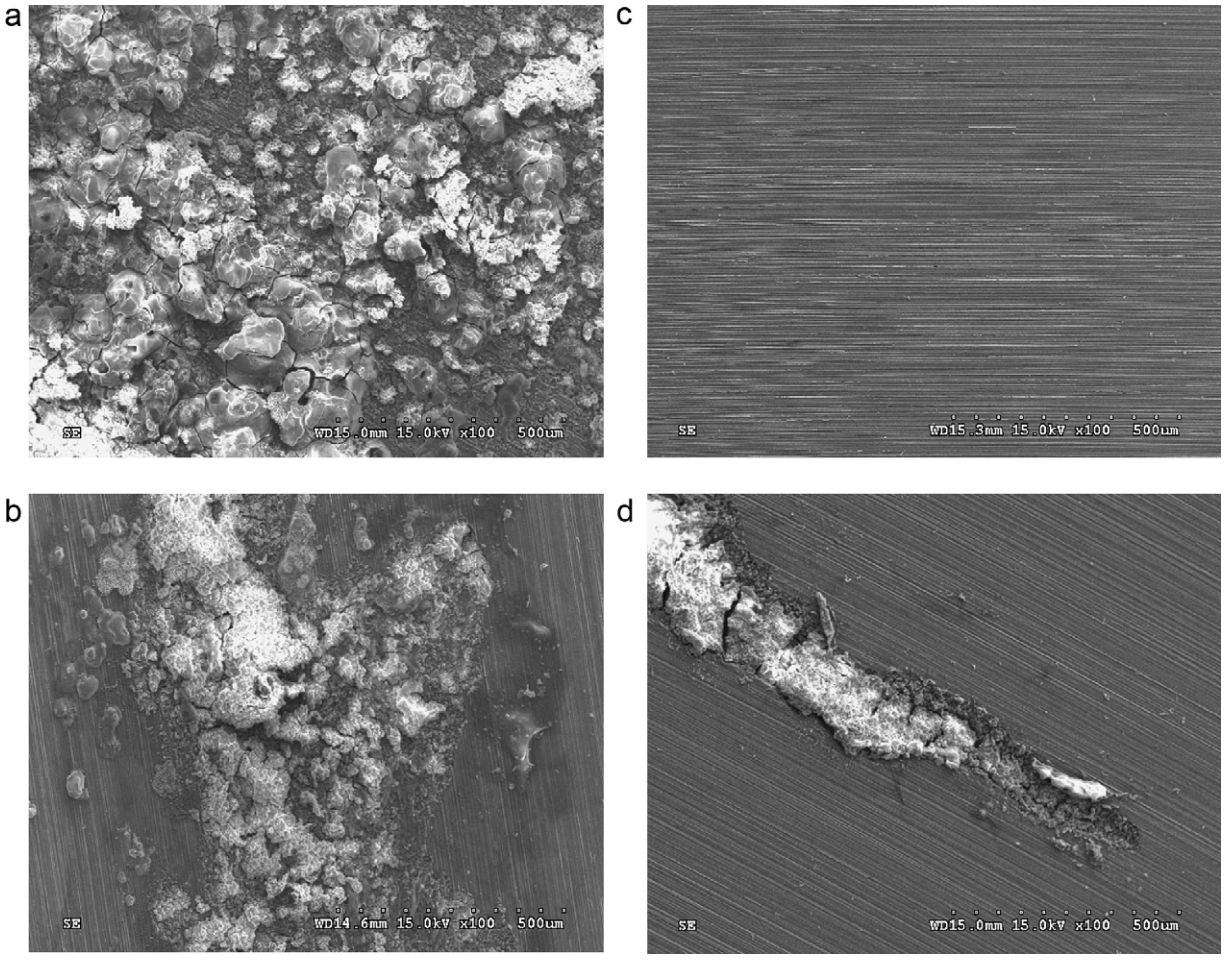

Fig. 11. SEM images of the specimens after the application of +800 mV_{SCE}.

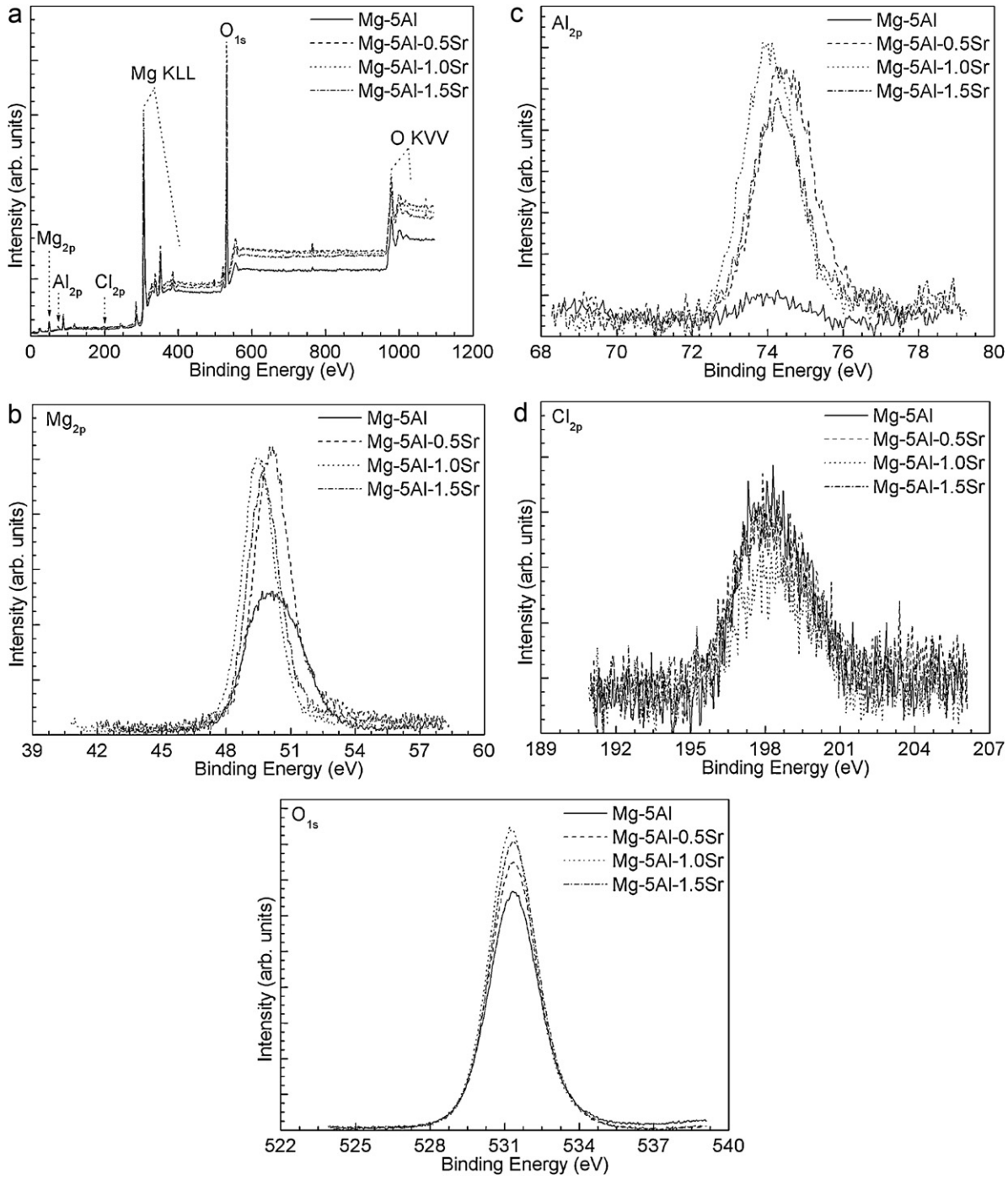

Fig. 12. XPS peak analysis for the surface products of the Mg–5Al–*x*Sr alloys: (a) survey scan spectra and narrow scan spectra of (b) Mg, (c) Al, (d) Cl and (e) O.

gests that the corrosion was quite serious and developed slowly in Fig. 11(b) and (d). The stability of the passive film observed with the addition of 1.0 wt% Sr corresponds to the results of the potentiodynamic polarization and potentiostatic tests.

The surface films were evaluated by XPS after applying a passive potential of $-900\,mV_{SCE}$ based on the data from the polarization curves. Fig. 12 shows the XPS spectra of the passive film. This figure shows peaks for Mg, Al, Cl and O. The peaks in the regions near 300 and 1100 eV were assigned to magnesium KLL and oxygen KVV [81,82]. Fig. 12(b)–(e) shows the narrow XP spectra for the Mg 2p, Al 2p, Cl 2p and O 1s regions, respectively. The Mg 2p and Al 2p spectra correspond to $Mg(OH)_2$ and $Al(OH)_3$ on the surface of the alloys. This figure also shows that the concentration of Al 2p and O 1s increased with increasing Sr content to 1.0 wt% Sr, and decreased with further increases in Sr content. In addition, a lower Cl peak was observed in the Mg–5Al–1.0Sr specimen. This suggests that the enriched Al product containing Mg played an important role in improving the surface film of a magnesium alloy, which impeded the adsorption of Cl^- ions.

4. Conclusions

1. The addition of Sr caused a decrease in the grain size of the α-Mg solid solution phase. Precipitation of the discontinuous $Mg_{17}Al_{12}$ phase at the grain boundaries was suppressed by the high density of Mg–Sr and Al–Sr compounds in the Sr-containing alloy.

The corrosion performance may be controlled by the microstructure with a higher density and more continuous precipitation around the finer α-Mg grains.

2. The pitting potential (E_{pit}) increased with increasing Sr content up to 1.0 wt% Sr, and decreased with further increases in Sr content. EIS showed that the semicircle was less depressed in the case of the Sr-containing specimens. The total resistance increased with increasing Sr content to 1.0 wt% Sr and decreased with further increases in Sr concentration.
3. Sr addition to Mg–5Al alloys facilitates the formation of an $Al(OH)_3$ passive film on the surface. In addition, the amount of chloride in the passive film decreases with increasing Sr content, indicating a more protective passive film on the Mg–5Al–1Sr alloy surface.

References

[1] A. Eliezer, J. Haddad, Y. Unigovski, E.M. Gutman, Mater. Manuf. Process. 20 (2005) 75–88.
[2] C. Blawert, N. Hort, K.U. Kainer, Trans. Indian Inst. Met. 57 (2004) 397–408.
[3] B. Viehweger, A. Karabet, M. During, L. Schaeffer, Mat.-wiss. u. Werkstofftech 36 (2005) 211–217.
[4] H. Friedrich, S. Schumann, J. Mater. Process. Technol. 117 (2001) 276–281.
[5] B.L. Mordike, T. Ebert, Mater. Sci. Eng. A302 (2001) 37–45.
[6] S. Schumann, H. Friedrich, in: B.L. Mordike, K.U. Kainer (Eds.), Magnesium Alloys and Their Application, Wolfsburg, Volkswagen, AG, 1998.
[7] J.E. Hillis, Light Met. Age 41 (1983) 25.
[8] S.R. Agnewa, J.F. Nie, Scripta Mater. 63 (2010) 671–673.
[9] E. Ghali, W. Dietzel, K.U. Kainer, J. Mater. Eng. Perform. 13 (2004) 7–23.
[10] G. Yan, W. Guixiang, D. Guojun, G. Fan, Z. Lili, Z. Milin, J. Alloys Compd. 463 (2008) 458–461.
[11] G.B. Hamu, D. Eliezer, L. Wagner, J. Alloys Compd. 468 (2009) 222–229.
[12] P. Shi, W.F. Ng, M.H. Wong, F.T. Cheng, J. Alloys Compd. 469 (2009) 286–292.
[13] X. Wang, X. Zeng, G. Wu, S. Yao, Y. Lai, J. Alloys Compd. 437 (2007) 87–92.
[14] Y. Liu, Q. Wang, Y. Song, D. Zhang, S. Yu, X. Zhu, J. Alloys Compd. 473 (2009) 550–556.
[15] N.D. Nam, J.G. Kim, K.S. Shin, H.C. Jung, Scripta Mater. 63 (2010) 625–628.
[16] X.M. Wang, X.Q. Zeng, G.S. Wu, S.S. Yao, Y.J. Lai, J. Alloys Compd. 456 (2008) 384–389.
[17] J. Zhang, J. Wang, X. Qiu, D. Zhang, Z. Tian, X. Niu, D. Tang, J. Meng, J. Alloys Compd. 464 (2008) 556–564.
[18] Y. Song, D. Shan, R. Chen, E.H. Han, Corros. Sci. 51 (2009) 1087–1094.
[19] G.L. Song, A. Atrens, Adv. Eng. Mater. 1 (1999) 11–33.
[20] E.P. Banczek, L.M.C. Zarpelon, R.N. Faria, I. Costa, J. Alloys Compd. 479 (2009) 342–347.
[21] J. Zhang, X. Niu, X. Qiu, K. Liu, C. Nan, D. Tang, J. Meng, J. Alloys Compd. 471 (2009) 322–330.
[22] W. Zhou, N.N. Aung, Y. Sun, Corros. Sci. 51 (2009) 403–408.
[23] G.L. Song, Corros. Sci. 51 (2009) 2063–2070.
[24] J. Zhang, Z. Leng, M. Zhang, J. Meng, Ruizhi Wu, J. Alloys Compd. 509 (2011) 1069–1078.
[25] Z. Wen, C. Wu, C. Dai, F. Yang, J. Alloys Compd. 488 (2009) 392–399.
[26] N. Liu, J. Wang, L. Wang, Y. Wu, L. Wang, Corros. Sci. 51 (2009) 1328–1333.
[27] N. Birbilis, M.K. Cavanaugh, A.D. Sudholz, S.M. Zhu, M.A. Easton, M.A. Gibson, Corros. Sci. 53 (2011) 168–176.
[28] E.N. El Sawy, H.A. El-Sayed, H.A. El Shayeb, J. Alloys Compd. 492 (2010) 69–76.
[29] W. Liu, F. Cao, A. Chen, L. Chang, J. Zhang, C. Cao, Corros. Sci. 52 (2010) 627–638.
[30] J. Zhang, K. Liu, D. Fang, X. Qiu, P. Yu, D. Tang, J. Meng, J. Alloys Compd. 480 (2009) 810–819.
[31] W. Liu, F. Cao, L. Chang, Z. Zhang, J. Zhang, Corros. Sci. 51 (2009) 1334–1343.
[32] K. Higashida, N. Narita, S. Asano, R. Onodera, Mater. Sci. Eng. A285 (2000) 111–121.
[33] K. Matsunaga, S. Ii, C. Iwamoto, T. Yamamoto, Y. Ikuhara, Nanotechnology 15 (2004) S376–S381.
[34] G.T. Bae, J.H. Bae, D.H. Kang, H. Lee, N.J. Kim, Met. Mater. Int. 15 (2009) 1–5.
[35] J. Du, J. Yang, M. Kuwabara, W. Li, J. Peng, J. Alloys Compd. 470 (2009) 134–140.
[36] X. Zhang, D. Kevorkov, M.O. Pekguleryuz, J. Alloys Compd. 501 (2010) 366–370.
[37] B. Nami, S.G. Shabestari, S.M. Miresmaeili, H. Razavi, Sh. Mirdamadi, J. Alloys Compd. 489 (2010) 570–575.
[38] B.S. Shin, J.W. Kwon, D.H. Bae, Met. Mater. Int. 15 (2009) 203–207.
[39] H.K. Lim, D.H. Kim, J.Y. Lee, W.T. Kim, D.H. Kim, J. Alloys Compd. 468 (2009) 308–314.
[40] J. Du, M. Wang, W. Li, J. Alloys Compd. 502 (2010) 74–79.
[41] B. Jiang, D. Qiu, M.X. Zhang, P.D. Ding, L. Gao, J. Alloys Compd. 492 (2010) 95–98.
[42] H. Guang, M. Guolong, L. Xiangfa, J. Alloys Compd. 486 (2009) 136–141.
[43] Q. Xiang, R.Z. Wu, M.L. Zhang, J. Alloys Compd. 477 (2009) 832–835.
[44] K. Liu, J. Zhang, G. Su, D. Tang, L.L. Rokhlin, F.M. Elkin, J. Meng, J. Alloys Compd. 481 (2009) 811–818.
[45] X.Y. Fang, D.Q. Yi, J.F. Nie, X.J. Zhang, B. Wang, L.R. Xiao, J. Alloys Compd. 470 (2009) 311–316.
[46] M. Shahzad, L. Wagner, J. Alloys Compd. 486 (2009) 103–108.
[47] D.H. Xiao, M. Song, F.Q. Zhang, Y.H. He, J. Alloys Compd. 484 (2009) 416–421.
[48] E.P. Kwon, K.D. Woo, S.H. Kim, D.S. Kang, K.J. Lee, J.Y. Jeon, Met. Mater. Int. 16 (2010) 701–707.
[49] H. Dong, L. Wang, Y. Wu, L. Wang, J. Alloys Compd. 506 (2010) 468–474.
[50] P. Lin, H. Zhou, W. Li, M. Wang, Q. Guo, H. Tang, Wei Li, J. Alloys Compd. 481 (2009) 373–378.
[51] M.M. Avedesian, H. Baker, Magnesium and Magnesium Alloys, ASTM International, The Materials Information Society, 1999.
[52] C.P. Liang, H.R. Gong, J. Alloys Compd. 489 (2010) 130–135.
[53] H. Dong, L. Wang, Y. Wu, L. Wang, J. Alloys Compd. 5069 (2010) 468–474.
[54] L. Shang, I.H. Jung, S. Yue, R. Verma, E. Essadiqic, J. Alloys Compd. 492 (2010) 173–183.
[55] J. Wang, R. Liao, L. Wang, Y. Wu, Z. Cao, L. Wang, J. Alloys Compd. 477 (2009) 341–345.
[56] L. Gao, R.S. Chen, E.H. Han, J. Alloys Compd. 481 (2009) 379–384.
[57] X. Tian, L.M. Wang, J.L. Wang, Y.B. Liu, J. An, Z.Y. Cao, J. Alloys Compd. 465 (2008) 412–416.
[58] W. Xiao, S. Jia, J. Wang, J. Wang, L. Wang, J. Alloys Compd. 458 (2008) 178–183.
[59] W. Xiao, S. Jia, J. Wang, Y. Wu, L. Wang, J. Alloys Compd. 480 (2009) L33–L36.
[60] S. González, I.A. Figueroa, I. Todd, J. Alloys Compd. 484 (2009) 612–618.
[61] M. Eddahbi, P. Perez, M.A. Monge, G. Garces, R. Pareja, P. Adeva, J. Alloys Compd. 473 (2009) 79–86.
[62] H.T. Son, J.S. Lee, D.G. Kim, K. Yoshimi, K. Maruyama, J. Alloys Compd. 473 (2009) 446–452.
[63] Z.P. Xu, G.Q. Lu, Chem. Mater. 17 (2005) 1055–1062.
[64] S.W. Jang, K.C. Shin, S.M. Lee, J. Ceram. Process. Res. 2 (2001) 189–192.
[65] J.H. Zhang, X.L. Zhoub, J.A. Wang, J. Mol. Catal. A: Chem. 247 (2006) 222–226.
[66] H.L. Lee, S.W. Nam, B.S. Hahn, J. Mater. Sci. 33 (1998) 5007–5014.
[67] S.S. Cho, B.S. Chun, C.W. Won, S.D. Kim, B.S. Lee, H. Baek, J. Mater. Sci. 34 (1999) 4311–4320.
[68] Y.J. Chung, J.L. Park, N.J. Kim, K.S. Shin, Mater. Sci. Forum 488–489 (2005) 845–848.
[69] Y.J. Chung, K.S. Shin, Mater. Sci. Forum 475–479 (2005) 537–540.
[70] H. Liu, Y. Chen, H. Zhao, S. Wei, W. Gao, J. Alloys Compd. 504 (2010) 345–350.
[71] J. Du, J. Yang, M. Kuwabara, W. Li, J. Peng, J. Alloys Compd. 470 (2009) 228–232.
[72] T. Wu, X.D. Peng, D.Y. Wang, W.D. Xie, Mater. Sci. Forum 610–613 (2009) 964–967.
[73] Y. Fan, G.H. Wu, C.Q. Zhai, Mater. Sci. Forum 546–549 (2007) 567–570.
[74] A.D. Sudholz, N. Birbilis, C.J. Bettles, M.A. Gibson, J. Alloys Compd. 471 (2009) 109–115.
[75] S.F. Liu, B. Li, X.H. Wang, W. Su, H. Han, J. Mater. Process. Technol. 209 (2009) 3999–4004.
[76] W. Xiaofeng, S. Yangshan, X. Feng, B. Jing, T. Weijian, Mater. Sci. Eng. A 508 (2009) 50–58.
[77] N. Jie-xin, C. Qiu-rong, X. Nai-xin, W. Zhong-ling, Trans. Nonferrous Met. Soc. China 18 (2008) 1058–1064.
[78] N.D. Nam, W.C. Kim, J.G. Kim, K.S. Shin, H.C. Jung, Corros. Sci. 51 (2009) 2942–2949.
[79] L. Gao, C. Zhang, M. Zhang, X. Huang, N. Sheng, J. Alloys Compd. 468 (2009) 285–289.
[80] J.R. Scully, D.C. Silverman, M.W. Kendig, Electrochemical Impedance—Analysis and Interpretation, ASTM STP 1188, ASTM, Philadelphia, PA, 1993, p. 54.
[81] X.M. Wang, X.Q. Zeng, Y. Zhou, G.S. Wu, S.S. Yao, Y.J. Lai, J. Alloys Compd. 460 (2008) 368–374.
[82] X. Zhong, Q. Li, J. Hu, Y. Lu, Corros. Sci. 50 (2008) 2304–2309.